Environmental Science and Pollution Research (2022) 29:45623–45634
https://doi.org/10.1007/s11356-022-19039-8

RESEARCH ARTICLE

Enhanced adsorptive removal of Cr(III) from the complex solution by NTA-modified magnetic mesoporous microspheres

Linqing Liang[1] · Jiahong Wang[1,2] · Xinhao Tong[1] · Shutong Zhang[1]

Received: 23 September 2021 / Accepted: 30 January 2022 / Published online: 11 February 2022
© The Author(s), under exclusive licence to Springer-Verlag GmbH Germany, part of Springer Nature 2022

Abstract

The Fe_3O_4@nSiO_2@mSiO_2/NTA (FNMs-NTA) was prepared by grafting magnetic mesoporous microspheres with nitrilotriacetic acid (NTA) and applied as an adsorbent for the removal of Cr(III) from complex solutions. Some characterization techniques including Brunauer–Emmett–Teller (BET), Fourier transform infrared spectrometer (FT-IR), X-ray diffraction (XRD), small-angle X-ray diffraction (SAXS), vibrating sample magnetometer (VSM), and thermal gravimetric analysis (TGA) were used to characterize functional groups and pore structure of FNMs-NTA, which proved that NTA was successfully decorated onto the magnetic Fe_3O_4@nSiO_2@mSiO_2 (FNMs) and FNMs-NTA featured a regular mesoporous structure. The batch adsorption of Cr(III) by FNMs-NTA exhibited high adsorption capacity (16.0 mg·g^{-1} at pH 3.0, and 25 °C). Adsorption data followed Freundlich isotherm and adsorption process was a spontaneous adsorption process. Moreover, the kinetics of adsorption were well explained by pseudo-second-order kinetic model. FNMs-NTA showed resistance to interfering inorganic cations (Na^+, Ca^{2+}) and complexing agents (EDTA). Furthermore, FNMs-NTA exhibited remarkable regeneration performance and easy separation under external magnetic field. X-ray photoelectron spectroscopy (XPS) analysis showed the FNMs-NTA had excellent adsorption ability for Cr(III) because of the ion exchange and surface complexation.

Keywords Nitrilotriacetic acid modified magnetic mesoporous microspheres · Cr(III) adsorption · High salt

Introduction

Industrial wastewater pollution discharged into the natural environment has caused serious pollution problems. In particular, heavy metal-polluted wastewater from industrial discharge has a serious impact on public health and ecosystems due to its bioaccumulation (Barakat 2011; Singh et al. 2015; Wu et al. 2016). Chromium is a typical heavy metal from tannery wastewater, usually produced during tanning stages, and mainly exists in the form of Cr(III) (Szalinska et al. 2010; Vilardi et al. 2018). Although Cr(III) is a necessary trace element for humans, a high concentration of Cr(III) is also harmful to humans and it can be easily oxidized to a higher toxic hexavalent state (Cr(VI)). In addition to the high content of Cr(III), a large amount of organic and inorganic ligands with good coordination ability can form stable complexes with Cr(III) in tanning wastewater (Jiraroj et al. 2006; Sillanpää et al. 2011), which makes Cr(III) removal from complex solution even more problematic. Therefore, how to efficiently remove Cr(III) from tanning wastewater has become particularly urgent.

Different strategies have been considered for the removal of Cr(III) to the upper acceptable limits, such as chemical precipitation (Duan et al. 2017), liquid–liquid extraction (Zhang et al. 2016), ion exchange (Manos and Kanatzidis 2016), electrochemical reduction (Meunier et al. 2006), and adsorption (Liu et al. 2019). Chemical precipitation is frequently applied for Cr(III) removal, while the presence of organic acids in complex effluent environment decreases the efficiency of chemical precipitation, while the residual complex Cr(III) with low concentration (2–10 mg·L^{-1}) needs to be removed to reach the discharge standards of China's Ministry of Environmental Protection for tanning wastewater

Responsible Editor: Tito Roberto Cadaval Jr.

I have not submitted my manuscript to a preprint server before submitting it to Environmental Science and Pollution Research.

✉ Jiahong Wang
wangjiahong@sust.edu.cn

[1] School of Environmental Science and Engineering, Shaanxi University of Science & Technology, Xi'an 710021, China

[2] Zhejiang Wenzhou Research Institute of Light Industry, Wenzhou 325003, Zhejiang, China

(Zhao and Chen 2019). Adsorption is widely used for heavy metal removal with low concentration because of its ease in operation, environment friendly, and cost-effectiveness (Pan et al. 2013; Wang et al. 2014). The most commonly applied adsorbents in water treatment are fly ash, bentonite, activated carbon, agricultural waste, and so on (Javed et al. 2018; Zaidi et al. 2018). However, some problems still exist for these adsorbents, such as difficulty of separation and regeneration in practical application, and the reduced adsorption capacity in a complex wastewater system. According to our previous study, the adsorption of Cr(III) by magnetic microsphere was inhibited in complex wastewater (Wang et al. 2020a), while for the magnetic mesoporous microsphere, negligible impact was observed for the adsorption of Cr(III) in high salinity wastewater (Wang et al. 2020b), which may be related to a mesoporous structure of adsorbent. Magnetic mesoporous microsphere is considered as a good carrier material for heavy metal wastewater treatment since it is cheap, chemically inert, and has a high surface area (Tu et al. 2016). What's more, nitrilotriacetic acid (NTA) can provide four coordination bonds for heavy metals, which form a stable chelate with metal ions (Mehta et al. 2015; Pastora et al. 2014).

In this study, Fe_3O_4@nSiO_2@mSiO_2/NTA (FNMs-NTA) was prepared by modification of magnetic mesoporous microspheres with NTA and investigated its potential ability to remove Cr(III) from complex solutions. The structures and physicochemical properties of FNMs-NTA were characterized by Brunauer–Emmett–Teller (BET), Fourier transform infrared spectrometer (FT-IR), X-ray diffraction (XRD), small-angle X-ray diffraction (SAXS), vibrating sample magnetometer (VSM), thermal gravimetric analysis (TGA), and X-ray photoelectron spectroscopy (XPS). The Cr(III) adsorption performance on FNMs-NTA were analyzed systematically, such as initial Cr(III) concentration, temperature, reaction time, solution pH, inorganic cations, and/or complexing agents (Na^+, Ca^{2+}, EDTA, NaCl, and EDTA), and adsorption mechanism was also advised based on the above results.

Materials and methods

Experimental reagents

NTA, pyridine, and N,N-dimethylformamide (DMF) were brought from Sinopharm Chemical Reagent Co. Ltd. Hexadecyl trimethyl ammonium bromide (CTAB) and (3-aminopropyl)trimethoxy silane (APTES) were provided by Sigma-Aldrich Co. Ltd. and Aladdin Reagent Co. Ltd., respectively. The remaining chemical reagents were offered by Tianjin Tianli Chemical Reagent Co. Ltd. All chemical reagents were analytical grade and the distilled water was used to conduct all experiments.

Preparation of the adsorbent

The preparation process of FNMs-NTA is shown in Fig. 1.

The magnetic mesoporous microspheres (FNMs) were prepared according to reference (Wang et al. 2020b). In order to synthesize nitrilotriacetic acid (NTAA), 2 g of NTA, 3 mL of pyridine, and 3 mL of DMF were mixed into a 50-mL flask, added 3 mL acetic anhydride (Ac_2O) drop by drop, and stirred vigorously at 65 °C for 24 h. Subsequently, 0.5 g of FNMs, 1.5 mL of APTES, and 3 mL of DMF were sequentially dissolved in the above solution. After stirring at 75 °C for 20 h, the samples were separated by the magnet, and then washed with Ac_2O, DMF, distilled water, saturated $NaHCO_3$ aqueous solution, distilled water, ethanol, and acetone, respectively. Finally, the samples were placed in a vacuum oven at 60 °C to dry overnight, resulting in FNMs-NTA (Chen et al. 2015).

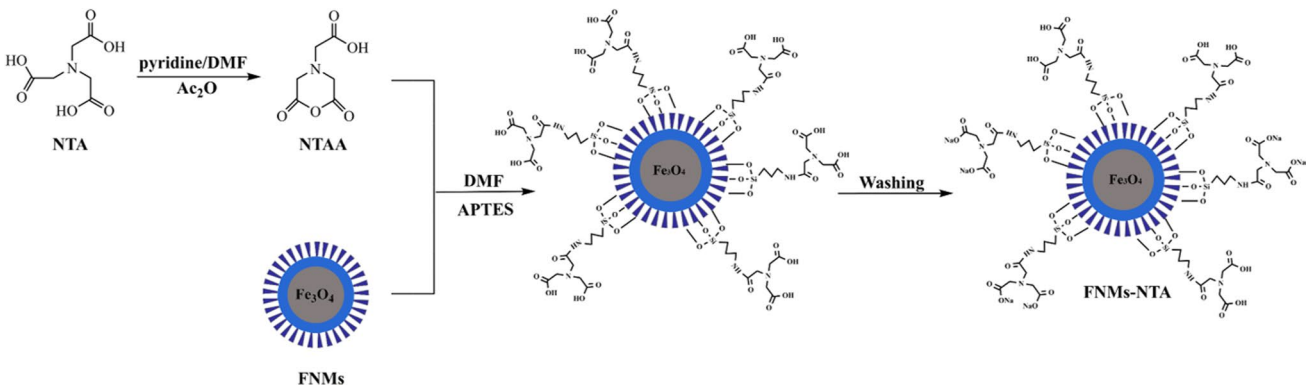

Fig. 1 Synthesis route for the preparation of FNMs-NTA

Characterization

BET (ASAP2460, Micromeritics Instrument Corp) was selected to measure the specific surface area, pore volume, and pore size distribution of samples. The phase composition and crystalline structure were analyzed by XRD and SAXS (Bruker D8, Bruker). The thermal stability was measured on a TGA (STA409PC, NETZSCH Group). FT-IR (Nexus 870, Nicolet) was used to examine the functional groups of a sample. The magnetic properties were analyzed by VSM (SQUID-VSM, America Quantum Design). XPS (AXUS SYPRA, Kratos) was performed to obtain the atomic composition of samples before and after FNM adsorption of Cr(III). The concentration of heavy metal ions in the solution was measured by ICP-OES (THEM, America).

Adsorption experiments

All the adsorption experiments in this study were carried out in a series of spiral glass tubes containing 20 mg of FNMs-NTA, 50 mL of Cr(III) solution (pH = 3.0) at 25 °C, and shaken at 170 r·min^{-1} for 6 h, except for the influence of temperature and contact time. The solution pH was adjusted with 1.0 M NaOH and HCl aqueous solution.

The influence of initial Cr(III) concentration on adsorption was studied by varying concentrations in the range of 2.5–50 mg·L^{-1} at 15, 25, and 35 °C. For the influence of contact time, 100 mg FNMs-NTA and 250 mL of (20, 50 mg·L^{-1}) Cr(III) solution were mixed and collected the sample at a certain time interval. Effects of pH were investigated by changing pH values from 2.0 to 9.0 in 20 mg·L^{-1} of Cr(III) solution. Na^+ and Ca^{2+} ions were selected as representatives to study the influence of inorganic cations; FNMs-NTA was added to the mixed solution, which was composed of Cr(III) (20 mg·L^{-1}) and Na^+, Ca^{2+} ions (10–60 mmol·L^{-1}). The influence of organic complexing agent was carried out in presence of EDTA and 10 mg·L^{-1} Cr(III) solution with a molar ratio of 0.5–20:1. For the influence of coexistence of inorganic cation and complexing agents, the mixed solution was prepared with Na^+ (300–2000 mg·L^{-1}) and the molar ration of Cr(III) (10 mg·L^{-1}) to EDTA was 1:1. The above experiments were performed on triplicates, and the errors should be within 5%.

To assess the regeneration performance of the saturated FNMs-NTA, the adsorption–desorption consecutive experiments were performed. After reaching adsorption equilibrium, the saturated FNMs-NTA was regenerated with 0.1 M HCl aqueous solution, washed 3 times with $NaHCO_3$ solution and distilled water, and then placed in a vacuum oven at 60 °C to dry. The experiment process was carried out 3 times repeatedly.

After the reaction was completed, the samples were taken and filtrated by 0.45 μm filter membrane, and determined the residual concentration of filtrate. The equilibrium adsorption amount for Cr(III) by FNMs-NTA was according to Eq. (1):

$$q_e = \frac{(C_0 - C_e)V}{m} \tag{1}$$

where q_e (mg·g^{-1}) is the equilibrium adsorption capacity, C_0 (mg·L^{-1}) and C_e (mg·L^{-1}) are the solution concentrations at initial and equilibrium, V (L) is the volume of solution, and m (g) is the quality of adsorbent.

Adsorption fitting model

The theoretical adsorption capacity and the distribution of Cr(III) molecules on FNMs-NTA were simulated by the Langmuir model and the Freundlich model.

The Langmuir model is displayed in Eq. (2):

$$\frac{1}{q_e} = \frac{1}{bq_{mC_e}} + \frac{1}{q_m} \tag{2}$$

The Freundlich model is represented as Eq. (3):

$$\ln q_e = \ln K_f + \frac{1}{n}\ln C_e \tag{3}$$

where q_m (mg·g^{-1}) is the theoretical maximum adsorption amount at equilibrium, b (L·mg^{-1}) is the adsorption equilibrium constant of Langmuir, and K_f and n are the characteristic constant and empirical constant of Freundlich.

The Gibbs–Helmholtz equation could be calculated thermodynamic parameters of FNMs-NTA to Cr(III), and analyzed the thermodynamic behavior during the adsorption process.

The Gibbs–Helmholtz equation is obtained by Eq. (4) and Eq. (5):

$$\Delta G^{\ominus} = \Delta H^{\ominus} - T\Delta S^{\ominus} \tag{4}$$

$$ln\frac{q_e}{C_e} = \frac{\Delta S^{\ominus}}{R} - \frac{\Delta H^{\ominus}}{RT} \tag{5}$$

where R (8.314 J·mol^{-1}·K^{-1}) is the molar gas constant, T (K) is temperature, ΔH^e (kJ·mol^{-1}), and ΔS^e (J·mol^{-1}·K^{-1}) and ΔG^e (kJ·mol^{-1}) are enthalpy, entropy, and Gibbs free energy, respectively.

The pseudo-first-order kinetic and pseudo-second-order kinetic could be analyzed the adsorption process of Cr(III) on FNMs-NTA.

The pseudo-first-order model is calculated by Eq. (6):

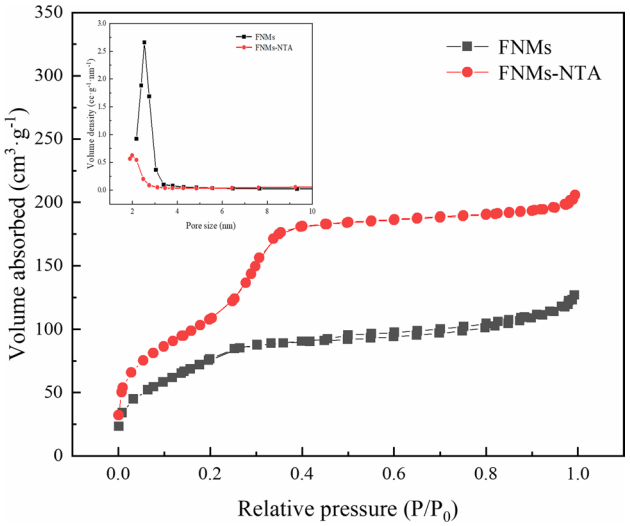

Fig. 2 N_2 adsorption/desorption isotherms and pore size distribution charts of FNMs and FNMs-NTA

Table 1 The surface and porosity characteristics of FNMs and FNMs-NTA

Sample	BET-specific surface ($m^2 \cdot g^{-1}$)	Pore volume ($cm^3 \cdot g^{-1}$)	Average pore diameter (nm)
FNMs	426.90	0.32	2.54
FNMs-NTA	293.63	0.15	2.18

$$\lg\left(q_e - q_t\right) = \lg q_e - k_1 t \tag{6}$$

The pseudo-second-order model is expressed by Eq. (7):

$$\frac{t}{q_t} = \frac{1}{k_2 q_e^2} + \frac{t}{q_e} \tag{7}$$

where t (min) is reaction time, q_t ($mg \cdot g^{-1}$) is the instantaneous adsorption amount, and k_1 (min^{-1}) and k_2 ($g \cdot mg^{-1} \cdot min^{-1}$) are the constant of pseudo-first-order kinetic and pseudo-second-order kinetic.

Results and discussion

Characterization

The nitrogen adsorption/desorption isotherms and the pore size distribution charts can be seen in Fig. 2. According to the IUPAC classification, the nitrogen adsorption/desorption isotherms of FNMs and FNMs-NTA fell into type IV, indicating that FNMs and FNMs-NTA had a strong interaction with nitrogen, and the adsorption process developed from mono-layer to multi-layer. In addition, the H1 hysteresis loop appeared in the latter part of the isotherms, which were related to mesoporous structure. As shown in Table 1, NTA modification could reduce the BET-specific surface area, pore volume, and average pore diameter, suggesting that the NTA entered into well-developed mesoporous channels of FNMs.

The wide-angle XRD patterns of FNMs and FNMs-NTA were analyzed by the powder samples (Fig. 3a). The characteristic diffraction peak of Fe_3O_4 appeared at $2\theta = 30.1°$, 35.4°, 43.1°, 53.5°, 57.0°, and 62.5°, respectively, corresponding to the crystal of (220), (331), (400), (422), (511), and (440) (Ren et al. 2013), which showed highly crystalline cubic spinel structure of FNMs. At $2\theta = 23°$, there was an amorphous SiO_2 diffraction peak, proving that SiO_2 coating was successfully formed. Owing to the NTA modification, the diffraction peaks ($2\theta = 23°$) of FNMs-NTA were weaker than FNMs (Yang et al. 2009). Moreover, a similar XRD pattern between FNMs and FNMs-NTA implied that the phase of FNMs did not change after surface functionalization of FNMs with NTA.

The SAXS patterns were presented in Fig. 3b. A characteristic peak of the hexagonal mesoporous structure at 2.26° (100) proved that the surface of the FNMs had an ordered mesoporous structure (Wang et al. 2010). However, the (100) peak of FNMs-NTA was weak, which because NTA entered the mesopores reducing the intensity of the diffraction peak.

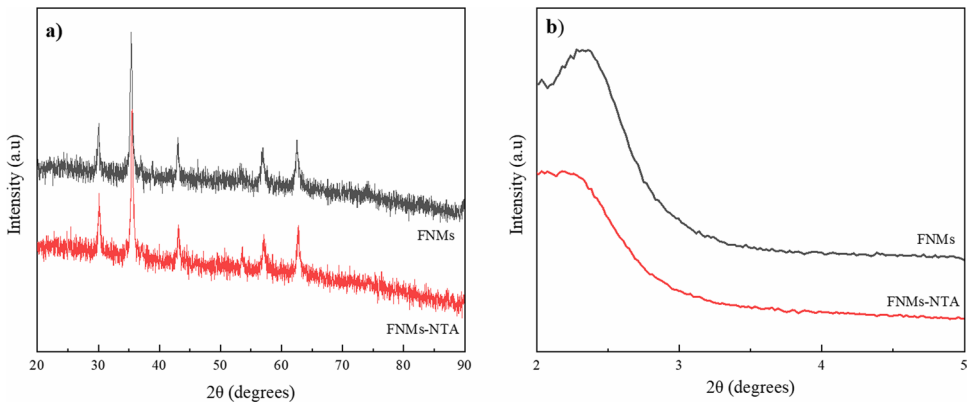

Fig. 3 Wide-angle XRD pattern (**a**) and SAXS pattern (**b**) of FNMs and FNMs-NTA

The thermogravimetric weight loss analysis of FNMs and FNMs-NTA is shown in Fig. 4, the weight loss of FNMs and FNMs-NTA were 26.5% and 37.03% as the temperature increased from 25 °C to 600 °C, respectively. The thermal weight loss between 25 °C and 200 °C was mainly attributed to the structural water escape. Nevertheless, the weight loss above 200 °C was mainly due to the decomposition of volatile inorganic and modified organics, especially silane molecules and carboxyl groups on the FNMs-NTA at 200–300 °C(Ren et al. 2013). Compared with FNMs, FNMs-NTA had a higher thermogravimetric weight loss, indicating that FNMs were successfully modified by NTA.

The FT-IR spectrum of FNMs (Fig. 5) displayed the existence of Fe–O (580 cm^{-1}), Si–O-Si (1078 cm^{-1} and 799 cm^{-1}), Si–OH (962 cm^{-1}) vibrations, and the -CH_2 vibration generated at 2800–3000 cm^{-1} due to the incomplete removal of the CTAB template from FNMs (Deng et al. 2008; Huang et al. 2012; Liu et al. 2016, 2017; Yang et al. 2009). In the spectrum of FNMs-NTA, the C = O stretching vibration peak appeared at 1406 cm^{-1}, which could be classified as a symmetrical carboxyl group or C-N bond, and another C = O stretching vibration peak appeared at 1631 cm^{-1} (Iqbal and Yun 2017; Liu et al. 2016, 2017; Singh et al. 2015). In comparison, the peak at 2800–3000 cm^{-1} disappeared in FNMs-NTA and proved that no CTAB was found in prepared FNMs-NTA material. Therefore, the change of the FT-IR spectrum confirmed that FNM surface were successfully modified by NTA.

The saturation magnetization was studied by magnetization curve, and the results are shown in Fig. 6. The saturation magnetization of FNMs and FNMs-NTA were 34.87 and 31.75 $emu \cdot g^{-1}$, respectively. In addition, the illustration displayed that the saturation magnetization of FNMs-NTA was decreased after NTA functionalization, but it still exhibits

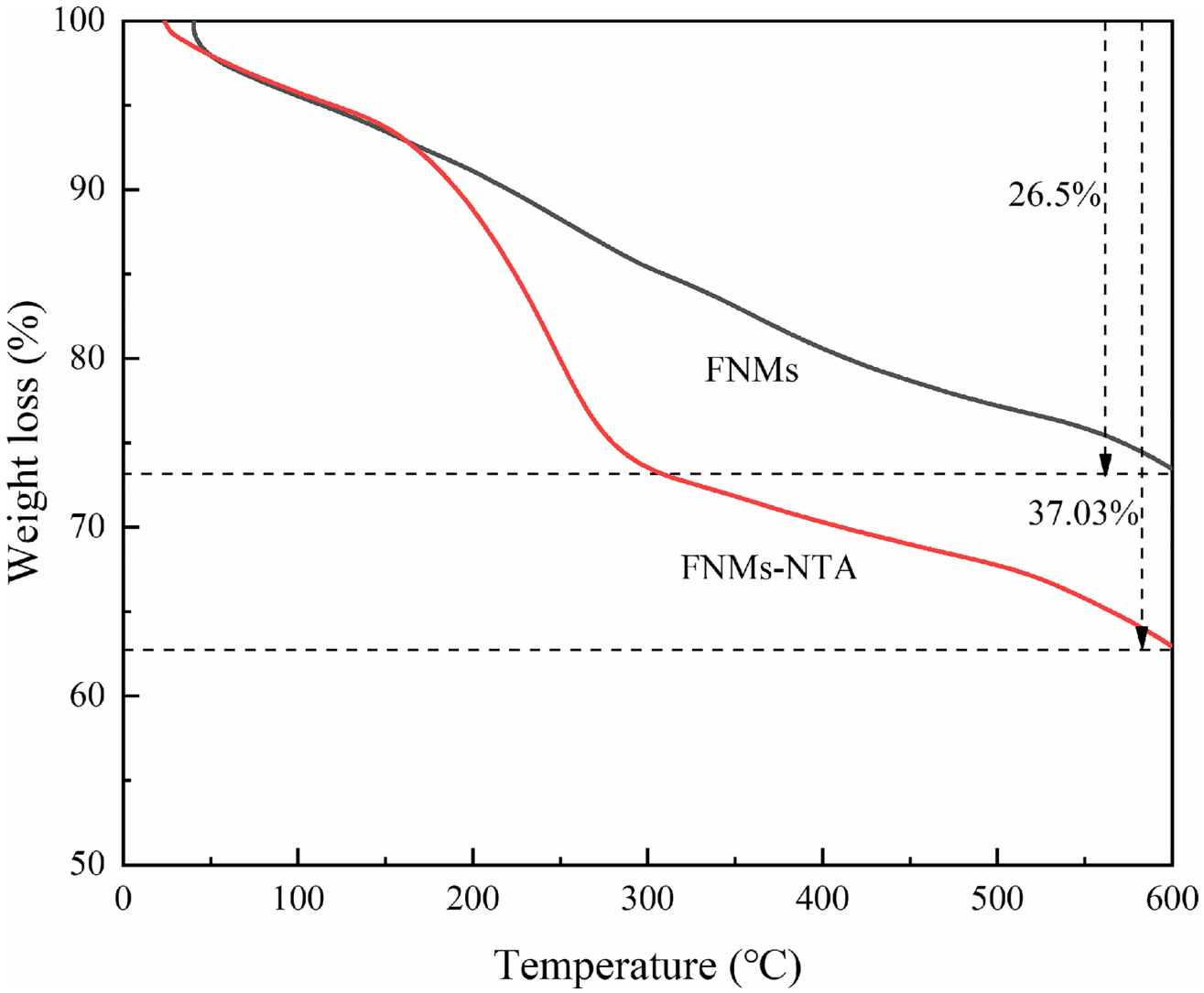

Fig.4 TGA curve of FNMs and FNMs-NTA

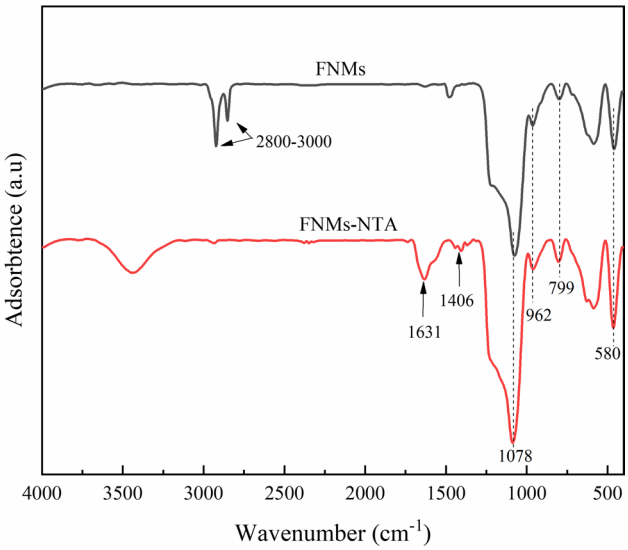

Fig.5 FT-IR spectra of FNMs and FNMs-NTA

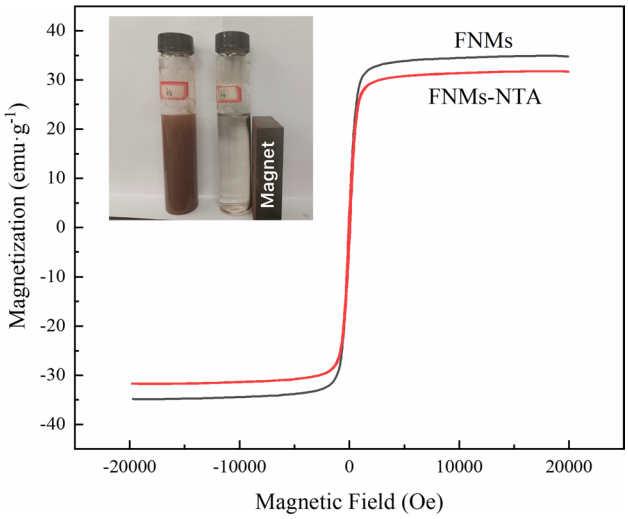

Fig.6 Magnetization curve of FNMs and FNMs-NTA

excellent magnetic properties, and could be quickly separated from the pollutants by applying a magnetic field.

The influence of solution pH

The state of heavy metal ions and the surface charge of FNMs-NTA are always influenced by solution pH (Singh et al. 2015). In the pH range of 2–9, the form distribution of Cr(III) is illustrated in Fig. 7a. When the pH was less than 3.0, the predominate Cr species were Cr(III); when the pH was about 4.0, the presence ratio of Cr^{3+} and $Cr(OH)^{2+}$ was dominant; when the pH was higher than 5.0, Cr(III) would precipitate as $Cr(OH)_3$ (Wang et al. 2013). The Cr(III) adsorption on FNMs-NTA at increasing solution pH is illustrated in Fig. 7b. The adsorption amount of FNMs-NTA on Cr(III) was increased rapidly in the pH range of 2.0 to 5.0, mainly because H^+ and Cr(III) were competing for active sites on the surface of FNMs-NTA (Repo et al. 2013, 2011). In addition, the amino group was protonated under acidic conditions (Juang and Ju 1997), and generated electrostatic repulsion with positively charged Cr^{3+}, $Cr(OH)_2^+$, and $Cr(OH)^{2+}$. The electrostatic attraction between Cr(III) and deprotonated FNMs-NTA increased at pH > 3, resulting in the increase of adsorption amount. However, the adsorption capacity had no significant change in the pH range of 6.0 to 9.0, which was mainly due to the formation of Cr(III) precipitation ($Cr(OH)_3$).

The influence of initial Cr(III) concentration

The results of FNMs and FNMs-NTA adsorbing different initial Cr(III) concentration at 25 °C are illustrated in Fig. 8. From the results, the Cr(III) adsorption amount increased remarkably after NTA modification, which was nearly 3 times that of FNMs. When the concentration of Cr(III) reached a certain value ($C_0 \geq 30$ mg·L^{-1}), there was no further adsorption site available for Cr(III) ions to occupy, indicating that FNMs-NTA attained saturation adsorption. In tested range, the maximum equilibrium adsorption amount

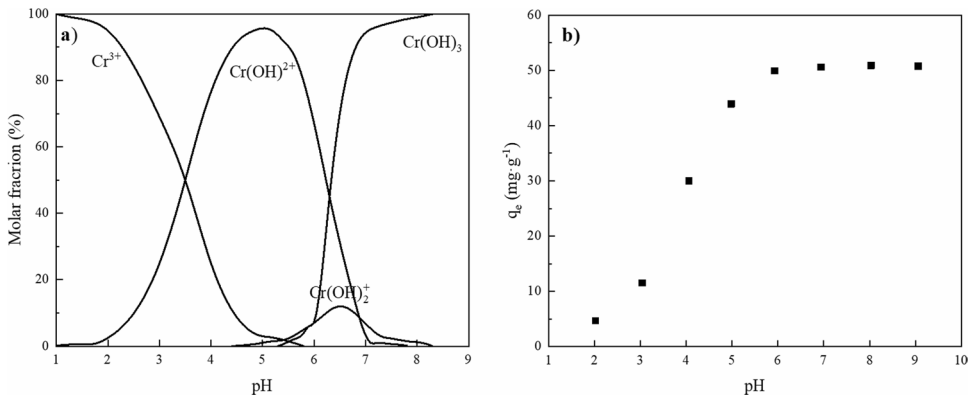

Fig.7 Cr(III) speciation diagram at different pH (**a**). The influence of reaction system pH on the adsorption of Cr(III) by FNMs-NTA (**b**)

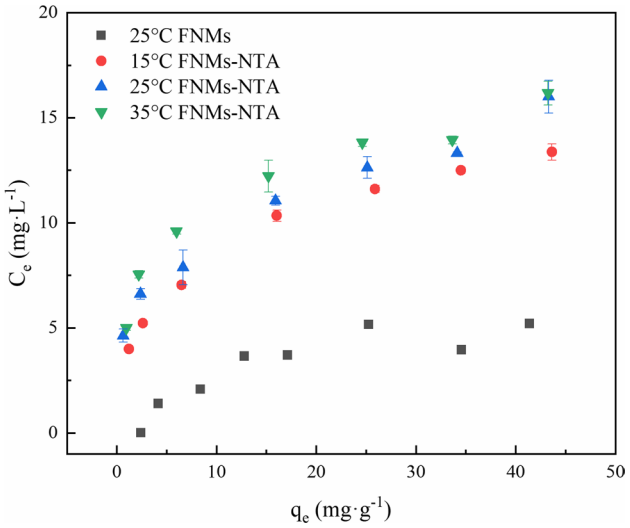

Fig. 8 The influence of initial concentration on adsorption of Cr(III) by FNMs at 25 °C and FNMs-NTA at 15, 25, and 35 °C

of FNMs and FNMs-NTA were 5.2 mg·g^{-1} and 16.00 mg·g^{-1} at 25 °C, respectively, which is comparable with other adsorbents tabulated in Table 2. The fitting parameters calculated by Freundlich model and Langmuir model are listed in Table 3. According to the R^2 values, the Freundlich model could simulate this adsorption process better than the Langmuir model, proving that the Cr(III) adsorption process was a multi-layer adsorption process. Besides, the $1/n = 0.282$ indicated that the surface of FNMs-NTA was heterogeneous (Cui et al. 2015).

The influence of temperature

Table 4 shows that the thermodynamic parameters for Cr(III) adsorption on FNMS-NTA were calculated from the Gibbs–Helmholtz equation. ΔG^e was a negative value and decreased with the increasing temperature, which indicated that the adsorption of Cr(III) by FNMs-NTA was a spontaneous process (Wang et al. 2021). The adsorption amount increased with the increase of temperature (Fig. 8), and ΔH^e and ΔS^e were positive value, proving that the adsorption process was an endothermic reaction, and increased the disorder of the solid–liquid system (Bai et al. 2020).

Table 3 The Langmuir and Freundlich model parameters of FNMs-NTA

Langmuir			Freundlich		
q_m (mg·g^{-1})	b (L·mg^{-1})	R^2	1/n	K_f (L·mg^{-1})	R^2
11.71	0.98	0.877	0.282	5.18	0.992

Table 4 The thermodynamic parameters for Cr(III) adsorption on FNMs-NTA

Temperature (°C)	ΔH^e (kJ·mol^{-1})	ΔS^e (J·mol^{-1}·K^{-1})	ΔG^e (kJ·mol^{-1})
15	31.85	114.64	−1.18
25	31.85	114.64	−2.33
35	31.85	114.64	−3.47

The influence of contact time

The influence of contact time on the adsorption of Cr(III) by FNMs-NTA is presented in Fig. 9. As it can be seen that initially, the adsorption of Cr(III) was rapid at 0–10 min. With the increase of contact time, the adsorption rate gradually slowed until it reached a stable state after 30 min. The kinetics parameters calculated are listed in Table 5. From the results, the correlation coefficient (R^2) of pseudo-second-order kinetic was up to 0.999, and the theoretical adsorption capacity of pseudo-second-order kinetic was consistent with the measured results. Hence, the pseudo-second-order kinetic could better fit the adsorption process, indicating that this process was caused by chemical adsorption. Moreover, the rate constant (k_2) decreased with the increase of the initial Cr(III) concentration, which might be due to the Cr(III) ions that were easily combined with adsorption sites on the surface of FNMs-NTA in low-concentration solutions.

Table 2 Comparison of Cr(III) adsorption properties with other adsorbents reported

Adsorbent	Temperature (°C)	pH	Adsorption capacity (mg·g^{-1})	Reference
Cinnamoyl C-phenylcalix[4] resorcinarene	30	7	0.5	(Budiana et al. 2021)
Activated carbon	25	5	12.2	(Mohan et al. 2006)
Attapulgite; Chitosan	25	5	10.97; 1.6	(Zou et al. 2011)
Cellulose-g-poly- nontmorillonite-based porous composites	20	2.46	9.58	(Hao et al. 2021)
FNMs-NTA	25	3	16.6	This study

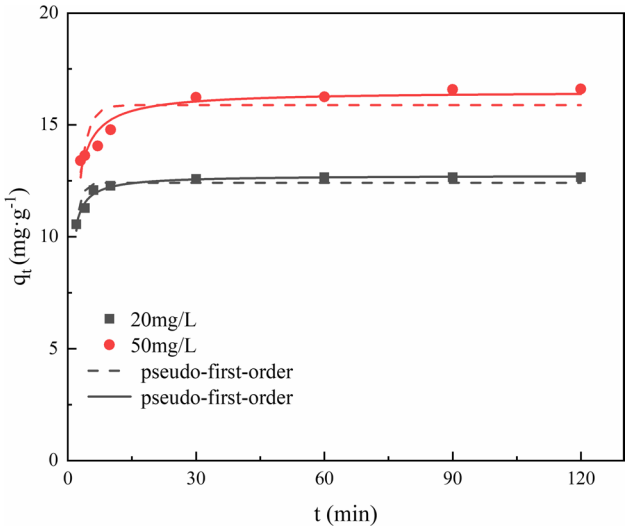

Fig. 9 The influence of reaction time on adsorption of Cr(III) by FNMs-NTA

The influence of inorganic cations and/or complexing agents

For the Cr(III) adsorption performance on FNMs-NTA in a complex system, the influence of inorganic cations, complexing agents, and the coexistence of complexing agents with high salty contents was investigated, respectively. The influence of coexisting inorganic cations (Na^+ and Ca^{2+}) on the adsorption process can be seen from Fig. 10a. Obviously, FNMs-NTA promoted the adsorption when Cr(III) ions coexisted with Na^+ or Ca^{2+}, proving that the adsorption amount increased with the increasing cation concentration. This might be the inactivated H^+ of the NTA function group that were replaced by the Na^+ and Ca^{2+} ions, resulting in more adsorption sites generated to promote adsorption (An et al. 2015).

The influence of increasing molar ratios of complexing agents (EDTA) to Cr(III) on the adsorption performance is displayed in Fig. 10b. Firstly, the slight promoting effect was observed at a low molar ratio of EDTA to Cr(III), which may be ascribed to Cr(III) combined with EDTA to form $[CrEDTA]^-$ and $[CrOHEDTA]^{2-}$ chelating with the amino groups on the surface of FNMs-NTA to promote Cr(III) adsorption (Liu et al. 2011; Zhang et al. 2019). Secondly, with the increasing molar ratio, the promotion effect weakened and gradually changed into the inhibiting effect. The adsorption capacity was reduced because the remaining EDTA would compete with Cr(III) for the active groups on the surface of FNMs-NTA. Even at a high molar ratio of Cr(III) to EDTA, the adsorbent still had a strong adsorption capacity for Cr(III).

Based on the above experiments, the influence of the coexistence of complexing agents with high salt on adsorption was explored. In the NaCl/EDTA/Cr(III) ternary-coexisting system (Fig. 10c), the removal of Cr(III) by FNMs-NTA was almost not affected by the presence of high salt system; contrarily, the adsorption performance was slightly promoted. Therefore, the synergy of EDTA and NaCl had little impact on the Cr(III) removal, which showed that the adsorbents could also have good potential for removing Cr(III) in complex environments.

Table 5 The pseudo-first-order kinetic and pseudo-second-order kinetic model parameters of FNMs-NTA

C_0 (mg·L^{-1})	q_e (mg·g^{-1})	Pseudo-first-order kinetic			Pseudo-second-order kinetic		
		k_1 (min^{-1})	q_e (mg·g^{-1})	R^2	k_2 (g·mg^{-1}·min^{-1})	q_e (mg·g^{-1})	R^2
20	12.65	4.52×10^{-2}	1.69	0.899	1.04×10^{-1}	12.71	0.999
50	16.60	3.7×10^{-3}	4.36	0.936	6.02×10^{-2}	16.67	0.999

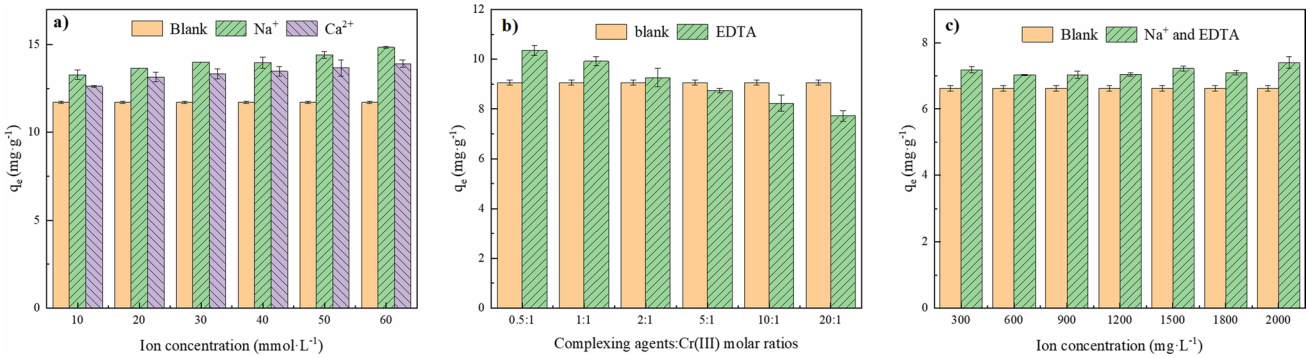

Fig. 10 The influence of inorganic cations concentration (**a**), the molar ratio of complexing agents to Cr(III) (**b**), and inorganic cations and complexing agents co-existing system (**c**) for Cr(III) adsorption onto FNMs-NTA

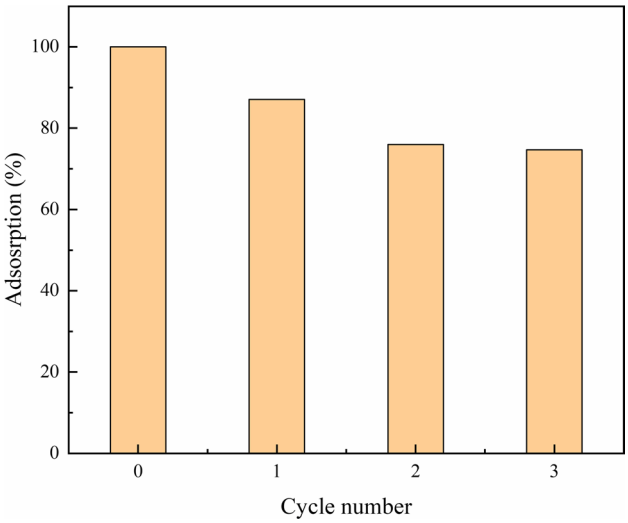

Fig.11 Cr(III) adsorption on original and regenerated FNMs-NTA

Regeneration of adsorbents

As the decreasing pH values, the adsorption performance of FNMs-NTA to Cr(III) was decreased. Hence, HCl solution (0.1 M) was selected as a desorption solvent to regenerate saturated FNMs-NTA. The adsorption performance of Cr(III) on regenerated FNMs-NTA is presented in Fig. 11. The regeneration test was conducted for 3 times, which were 87.01%, 75.97%, and 74.69% of the original adsorption capacity, respectively. The reduced adsorption amount after the first regeneration was that Cr(III) could not be completely desorbed from FNMs-NTA. The second and third regeneration test showed no significantly decrease, indicating that the regenerated FNMs-NTA still had prominent adsorption for low concentration of Cr(III), and the adsorbent had excellent repeatability in practical application.

Table 6 Binding energy and relative content (%) of C 1 s for FNMs-NTA and FNMs-NTA-Cr(III)

Valance state	Component	FNMs-NTA		FNMs-NTA-Cr(III)	
		Binding energy (eV)	Relative contents (%)	Binding energy (eV)	Relative contents (%)
C 1 s	C–C	284.5	55.22	284.6	55.82
	C-O	285.6	35.40	285.8	32.28
	C=O	288.6	9.38	288.6	11.90

Adsorption mechanism

To research the adsorption process of Cr(III) in more detail, the XPS analysis was performed on FNMs-NTA and after FNMs-NTA adsorbed Cr(III) (FNMs-NTA-Cr(III)). The wide scan spectra and Na 1 s spectra of before and after Cr(III) adsorption are illustrated in Fig. 12a–b, respectively. The Si 2p peak at 102.4 eV could be detected before and after Cr(III) adsorption, but the iron (Fe) peak could not be detected, indicating that the surface of FNMs-NTA is covered by an amorphous SiO_2 shell, and X-rays could not penetrate this shell (Yang et al. 2009). The Cr 2p peak that appeared in the wide scan spectra of FNMs-NTA-Cr(III) could be separated into Cr 2p1/2 (587 eV) and Cr 2p3/2 (577 eV), which demonstrated that Cr(III) was successfully adsorbed onto the FNMs-NTA surface. Compared before and after Cr(III) adsorption, the Na 1 s peak at 1071 eV disappeared in FNMs-NTA-Cr(III), mainly because the Na^+ on the surface of FNMs-NTA participated in ions exchange with Cr(III) (Liu et al. 2011).

The C 1 s spectra of FNMs-NTA and FNMs-NTA-Cr(III) are presented in Fig. 12c; the C 1 s was composed of the aliphatic group (C–C), a hydroxyl group (C-O), and carbonyl group (C=O); and their binding energies were 284.5, 285.8, and 288.4 eV, respectively, which belonged to the NTA

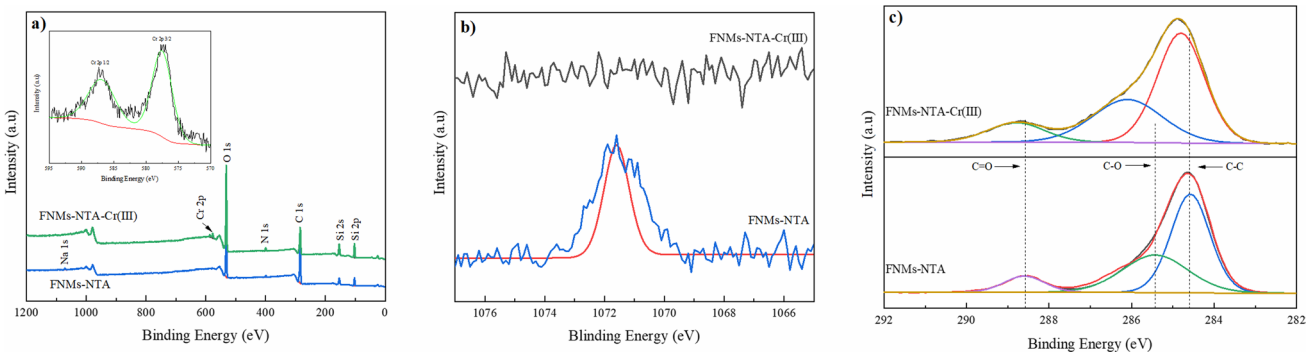

Fig.12 XPS spectra (**a**), Na 1 s spectra (**b**), and C1s spectra (**c**) of FNMs-NTA and FNMs-NTA-Cr(III)

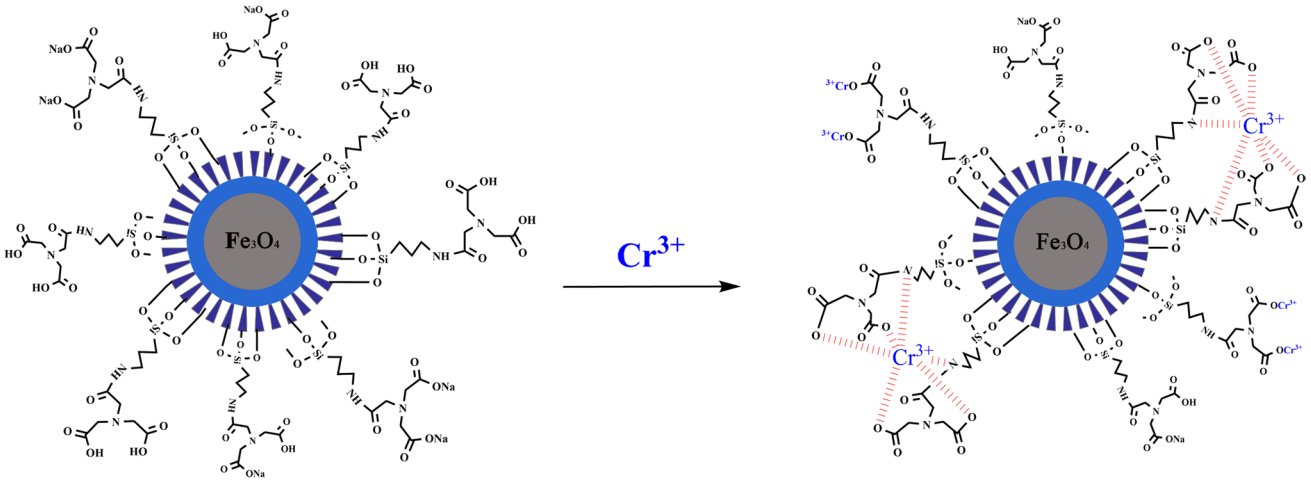

Fig.13 Adsorption mechanism of Cr(III) on FNMs-NTA

functional groups on FNMs-NTA (Lim et al. 2008). The binding energy and relative content (%) of C 1 s for FNMs-NTA and FNMs-NTA-Cr(III) are summarized in Table 6. After FNMs-NTA bounded Cr(III), the relative content of the hydroxyl groups of the adsorbent decreased, while the relative content of the carbonyl group increased, indicating that the combination of Cr(III) with FNMs-NTA led to the hydroxyl group of single bond that disappeared. Meanwhile, Cr(III) ions were removed by complexation with the NTA functional groups of FNMs-NTA (Zheng et al. 2009). Combining the experimental results and characterization analysis, it was concluded that the adsorption mechanisms included ion exchange and the surface complexation of FNMs-NTA functional groups (Fig. 13).

Conclusions

Magnetic mesoporous microspheres modified by NTA (FNMs-NTA) were successfully prepared. A variety of characterization results demonstrated that FNMs-NTA was a magnetic mesoporous material, and NTA was successfully decorated onto the surface of FNMs. The Cr(III) adsorption was a spontaneous process, and conformed to the Freundlich model and the pseudo-second-order kinetic model. The superior adsorption performance was due to ion exchange and surface complexation. At the same time, FNMs-NTA could still exhibit excellent Cr(III) adsorption capacity under the interference of inorganic cations and/or complexing agents, as well as remarkable separation and regeneration performance. Thus, compared with other adsorbents, NTA-modified magnetic mesoporous microspheres can be used to adsorb Cr(III) from a complex solution.

Author contribution LL did some of adsorption experiments, analyzed the data, and edited the manuscript; JW conceived the research, edited the manuscript, and supervised the project; XT did some of adsorption experiments, and reviewed the manuscript; SZ did data curation, and reviewed the manuscript.

Funding We are thankful for the financial supports provided by National Natural Science Foundation of China (22076111,21677092), and also thankful for the Basic Research Program Funded by Wenzhou (S20180009), China.

Availability of data and materials The data used and/or analyzed during the current study are available from the corresponding author on reasonable request.

Declarations

Ethics approval and consent to participate Not applicable.

Consent for publication Not applicable.

Competing interests The authors declare no competing interests.

References

An B, Lee H, Lee S, Lee S, Choi J (2015) Determining the selectivity of divalent metal cations for the carboxyl group of alginate hydrogel beads during competitive sorption. J Hazard Mater 298:11–18. https://doi.org/10.1016/j.jhazmat.2015.05.005

Bai C, Wang L, Zhu Z (2020) Adsorption of Cr(III) and Pb(II) by graphene oxide/alginate hydrogel membrane: characterization, adsorption kinetics, isotherm and thermodynamics studies. Int J Biol Macromol 147:898–910. https://doi.org/10.1016/j.ijbiomac.2019.09.249

Barakat MA (2011) New trends in removing heavy metals from industrial wastewater. Arabian J Chem 4:361–377. https://doi.org/10.1016/j.arabjc.2010.07.019

Budiana IGMN, Jasman J, Neolaka YAB, Riwu AAP, Elmsellem H, Darmokoesoemo H, Kusuma HS (2021) Synthesis,

characterization and application of cinnamoyl C-phenylcalix[4] resorcinarene (CCPCR) for removal of Cr(III) ion from the aquatic environment. J Mol Liq 324:114776. https://doi.org/10.1016/j.molliq.2020.114776

Chen F, Hong M, You W, Li C, Yu Y (2015) Simultaneous efficient adsorption of Pb^{2+} and MnO_4 ions by MCM-41 functionalized with amine and nitrilotriacetic acid anhydride. Appl Surf Sci 357:856–865. https://doi.org/10.1016/j.apsusc.2015.09.069

Cui L, Wang Y, Gao L, Hu L, Yan L, Wei Q, Du B (2015) EDTA functionalized magnetic graphene oxide for removal of Pb(II), Hg(II) and Cu(II) in water treatment: adsorption mechanism and separation property. Chem Eng J 281:1–10. https://doi.org/10.1016/j.cej.2015.06.043

Deng Y, Qi D, Deng C, Zhang X, Zhao D (2008) Superparamagnetic high-magnetization microspheres with an Fe_3O_4@SiO_2 core and perpendicularly aligned mesoporous SiO_2 shell for removal of microcystins. J Am Chem Soc 130:28–29. https://doi.org/10.1021/ja0777584

Duan W, Chen G, Chen C, Sanghvi R, Iddya A, Walker S, Liu H, Ronen A, Jassby D (2017) Electrochemical removal of hexavalent chromium using electrically conducting carbon nanotube/polymer composite ultrafiltration membranes. J Membr Sci 531:160–171. https://doi.org/10.1016/j.memsci.2017.02.050

Hao X, Tao E, Yang S, Li Y (2021) A new montmorillonite-based porous composites: effectively removal of Cr(III)-organic complexes in tannery wastewater. J Polym Environ. https://doi.org/10.1007/s10924-021-02193-4

Huang J, Ye M, Qu Y, Chu L, Chen R, He Q, Xu D (2012) Pb (II) removal from aqueous media by EDTA-modified mesoporous silica SBA-15. J Colloid Interface Sci 385:137–146. https://doi.org/10.1016/j.jcis.2012.06.054

Iqbal S, Yun JI (2017) EDTA-functionalized mesoporous silica for the removal of corrosion products: adsorption studies and performance evaluation under gamma irradiation. Micropor Mesopor Mater 248:149–157. https://doi.org/10.1016/j.micromeso.2017.04.028

Javed HS, Zahir K, Abdul A, Atif S, Mansha M (2018) Adsorption of mordant red 73 dye on acid activated bentonite: kinetics and thermodynamic study. J Mol Liq 254:398–405. https://doi.org/10.1016/j.molliq.2018.01.100

Jiraroj D, Unob F, Hagège A (2006) Degradation of Pb–EDTA complex by a H_2O_2/UV process. Water Res 40:107–112. https://doi.org/10.1016/j.watres.2005.10.041

Juang R, Ju C (1997) Equilibrium sorption of Copper(II)−ethylenediaminetetraacetic acid chelates onto cross-linked, polyaminated chitosan beads. Ind Eng Chem Res 36:5403–5409. https://doi.org/10.1021/ie970322k

Lim S, Zheng Yu, Zou S, Chen JP (2008) Characterization of copper adsorption onto an alginate encapsulated magnetic sorbent by a combined FT-IR, XPS, and mathematical modeling study. Environ Sci Technol 42:2551. https://doi.org/10.1021/es7021889

Liu L, Liu J, Lu Z, Yang Z, Lv C, Xue J, Tang A (2019) Synthesis and characterization of magnetic Fe_3O_4@$CaSiO_3$ composites and evaluation of their adsorption characteristics for heavy metal ions. Environ Sci Pollut Res Int 26:8721–8736. https://doi.org/10.1007/s11356-019-04352-6

Liu W, Zeng F, Jiang H, Zhang X (2011) Adsorption of lead (Pb) from aqueous solution with Typha angustifolia biomass modified by $SOCl_2$ activated EDTA. Chem Eng J 170:21–28. https://doi.org/10.1016/j.cej.2011.03.020

Liu Y, Fu R, Sun Y, Zhou X, Baig SA, Xu X (2016) Multifunctional nanocomposites Fe_3O_4@SiO_2-EDTA for Pb(II) and Cu(II) removal from aqueous solutions. Appl Surf Sci 369:267–276. https://doi.org/10.1016/j.apsusc.2016.02.043

Liu Y, Lou Z, Sun Y, Zhou X, Baig SA, Xu X (2017) Influence of complexing agent on the removal of Pb(II) from aqueous solutions by modified mesoporous SiO_2. Micropor Mesopor Mater 246:1–13. https://doi.org/10.1016/j.micromeso.2017.03.005

Manos MJ, Kanatzidis MG (2016) Metal sulfide Ion exchangers: superior sorbents for the capture of toxic and nuclear waste-related metal ions. Chem Sci 7:4804–4824. https://doi.org/10.1002/chin.201638242

Mehta D, Mazumdar S, Singh SK (2015) Magnetic adsorbents for the treatment of water/wastewater—a review. Journal of Water Process Engineering 7:244–265. https://doi.org/10.1016/j.jwpe.2015.07.001

Meunier N, Drogui P, Montané C, Hausler R, Mercier G, Blais JF (2006) Comparison between electrocoagulation and chemical precipitation for metals removal from acidic soil leachate. J Hazard Mater 137:581–590. https://doi.org/10.1016/j.jhazmat.2006.02.050

Mohan D, Singh KP, Singh VK (2006) Trivalent chromium removal from wastewater using low cost activated carbon derived from agricultural waste material and activated carbon fabric cloth. J Hazard Mater 135:280–295. https://doi.org/10.1016/j.jhazmat.2005.11.075

Pan J, Jiang J, Xu R (2013) Adsorption of Cr(III) from acidic solutions by crop straw derived biochars. J Environ Sci 25:1957–1965. https://doi.org/10.1016/S1001-0742(12)60305-2

Pastora JG, Bringas E, Ortiz I (2014) Recent progress and future challenges on the use of high performance magnetic nano-adsorbents in environmental applications. Chem Eng J 256:187–204. https://doi.org/10.1016/j.cej.2014.06.119

Ren Y, Abbood HA, He F, Peng H, Huang K (2013) Magnetic EDTA-modified chitosan/SiO_2/Fe_3O_4 adsorbent: preparation, characterization, and application in heavy metal adsorption. Chem Eng J 226:300–311. https://doi.org/10.1016/j.cej.2013.04.059

Repo E, Warchoł JK, Bhatnagar A, Sillanpää M (2011) Heavy metals adsorption by novel EDTA-modified chitosan–silica hybrid materials. J Colloid Interface Sci 358:261–267. https://doi.org/10.1016/j.jcis.2011.02.059

Repo E, Warchoł JK, Bhatnagar A, Mudhoo A, Sillanpää M (2013) Aminopolycarboxylic acid functionalized adsorbents for heavy metals removal from water. Water Res 47:4812–4832. https://doi.org/10.1016/j.watres.2013.06.020

Sillanpää MET, Agustiono Kurniawan T, Lo W (2011) Degradation of chelating agents in aqueous solution using advanced oxidation process (AOP). Chemosphere 83:1443–1460. https://doi.org/10.1016/j.chemosphere.2011.01.007

Singh D, Verma S, Gautam RK, Krishna V (2015) Copper adsorption onto synthesized nitrilotriacetic acid functionalized Fe_3O_4 nanoparticles: kinetic, equilibrium and thermodynamic studies. J Environ Chem Eng 3:2161–2171. https://doi.org/10.1016/j.jece.2015.07.020

Szalinska E, Dominik J, Vignati DAL, Bobrowski A, Bas B (2010) Seasonal transport pattern of chromium(III and VI) in a stream receiving wastewater from tanneries. Appl Geochem 25:116–122. https://doi.org/10.1016/j.apgeochem.2009.11.002

Tu J, Boyle AL, Friedrich H, Bomans P, Bussmann J, Sommerdijk N, Jiskoot W, Kros A (2016) Mesoporous silica nanoparticles with large pores for the encapsulation and release of proteins. ACS Appl Mater Interfaces 8:32211–32219. https://doi.org/10.1021/acsami.6b11324

Vilardi G, Di Palma L, Verdone N (2018) On the critical use of zero valent iron nanoparticles and Fenton processes for the treatment of tannery wastewater. Journal of Water Process Engineering 22:109–122. https://doi.org/10.1016/j.jwpe.2018.01.011

Wang J, Zheng S, Liu J, Xu Z (2010) Tannic acid adsorption on amino-functionalized magnetic mesoporous silica. Chem Eng J 165:10–16. https://doi.org/10.1016/j.cej.2010.08.066

Wang J, Atif S, Zhang D (2020a) Adsorption of Cr(III) by EGTA modified magnetic microsphere: effect of high salinity and organic chelating acids. Environ Technol Innovation 20:101088. https://doi.org/10.1016/j.eti.2020.101088

Wang J, Tong X, Chen Y, Sun T, Wang C (2020b) Enhanced removal of Cr(III) in high salt organic wastewater by EDTA modified magnetic mesoporous silica. Micropor Mesopor Mater 303:110262. https://doi.org/10.1016/j.micromeso.2020.110262

Wang T, Liu W, Xiong L, Xu N, Ni J (2013) Influence of pH, ionic strength and humic acid on competitive adsorption of Pb(II), Cd(II) and Cr(III) onto titanate nanotubes. Chem Eng J 215–216:366–374. https://doi.org/10.1016/j.cej.2012.11.029

Wang T, Jin X, Chen Z, Megharaj M, Naidu R (2014) Simultaneous removal of Pb(II) and Cr(III) by magnetite nanoparticles using various synthesis conditions. J Ind Eng Chem 20:3543–3549. https://doi.org/10.1016/j.jiec.2013.12.047

Wang Z, Jia Y, Song W, Li X, Xu K, Wang Z (2021) Optimization of boron adsorption from desalinated seawater onto UiO-66-NH_2/GO composite adsorbent using response surface methodology. J Clean Prod 300:126974. https://doi.org/10.1016/j.jclepro.2021.126974

Wu X, Cobbina SJ, Mao G, Xu H, Zhang Z, Yang L (2016) A review of toxicity and mechanisms of individual and mixtures of heavy metals in the environment. Environ Sci Pollut Res 23:8244–8259. https://doi.org/10.1007/s11356-016-6333-x

Yang P, Quan Z, Hou Z, Li C, Kang X, Cheng Z, Lin J (2009) A magnetic, luminescent and mesoporous core–shell structured composite material as drug carrier. Biomaterials 30:4786–4795. https://doi.org/10.1016/j.biomaterials.2009.05.038

Zaidi N, Lim L, Usman A (2018) Artocarpus odoratissimus leaf-based cellulose as adsorbent for removal of methyl violet and crystal violet dyes from aqueous solution. Cellulose 25:1–13. https://doi.org/10.1007/s10570-018-1762-y

Zhang G, Chen D, Zhao W, H, Wang, L, T, (2016) A novel D_2EHPA-based synergistic extraction system for the recovery of chromium (III). Chem Eng J 302:233–238. https://doi.org/10.1016/j.cet.2016.05.063

Zhang X, Huang P, Zhu S, Hua M, Pan B (2019) Nanoconfined hydrated Zirconium oxide for selective removal of Cu(II)-carboxyl complexes from high-salinity water via ternary complex formation. Environ Sci Technol 53:5319–5327. https://doi.org/10.1021/acs.est.9b00745

Zhao C, Chen W (2019) A review for tannery wastewater treatment: some thoughts under stricter discharge requirements. Environ Sci Pollut Res 26:26102–26111. https://doi.org/10.1007/s11356-019-05699-6

Zheng J, Feng H, Lam MH, Lam PK, Ding Y, Yu H (2009) Removal of Cu(II) in aqueous media by biosorption using water hyacinth roots as a biosorbent material. J Hazard Mater 171:780–785. https://doi.org/10.1016/j.jhazmat.2009.06.078

Zou X, Pan J, Ou H, Wang X, Guan W, Li C, Yan Y, Duan Y (2011) Adsorptive removal of Cr(III) and Fe(III) from aqueous solution by chitosan/attapulgite composites: Equilibrium, thermodynamics and kinetics. Chem Eng J 167:112–121. https://doi.org/10.1016/j.cej.2010.12.009

Publisher's note Springer Nature remains neutral with regard to jurisdictional claims in published maps and institutional affiliations.